Interpretation of the magnetic resonance data and their use in computational fluid dynamics

H. Švihlová[a], A. Jarolímová[a], J. Hron[a], R. Chabiniok[b,c], K. R. Rajagopal[d], J. Málek[a], and K. Rajagopal[e]

a, Faculty of Mathematics and Physics, Mathematical Institute, Charles University, Czech Republic

b, Department of Pediatrics, UT Southwestern Medical Center, Dallas, TX; Inria Saclay Ile-de-France, France

c, LMS, Ecole Polytechnique, Institut Polytechnique de Paris, France; St Thomas' Hospital, King's College London, UK

d, Texas A&M University, College Station TX, United States

e, Memorial Hermann Texas Medical Center, Houston TX, United States

The presentation is based on the following study:

- H. Švihlová, J. Hron, J. Málek, K. R. Rajagopal, K. Rajagopal (2016): *Determination of pressure data from velocity data with a view toward its application in cardiovascular mechanics. Part 1. Theoretical considerations.* In: International Journal of Engineering Science 105,108–127.
- H. Švihlová, J. Hron, J. Málek, K. R. Rajagopal, K. Rajagopal (2017): *Determination of pressure data from velocity data with a view towards its application in cardiovascular mechanics. Part 2: A study of aortic valve stenosis.* In: International Journal of Engineering Science 114,1–15.
- H. Švihlová, A. Jarolímová, J. Hron, R. Chabiniok, B. Piekarski, S. M. Emani, K. R. Rajagopal, J. Málek, K. Rajagopal (2020): *The impact of blood-aortic root boundary slip conditions on aortic root vorticity.* comming soon.

The work was supported by GAČR project 18-12719S and AZV ČR grant no. 17-32872A and no. NV19-04-00270.

Aortic valve stenosis evaluation

Aortic root physiological flow

The impact of slip boundary conditions on aortic root vorticity

Aortic valve stenosis evaluation

Aortic root physiological flow

The impact of slip boundary conditions on aortic root vorticity

Valves

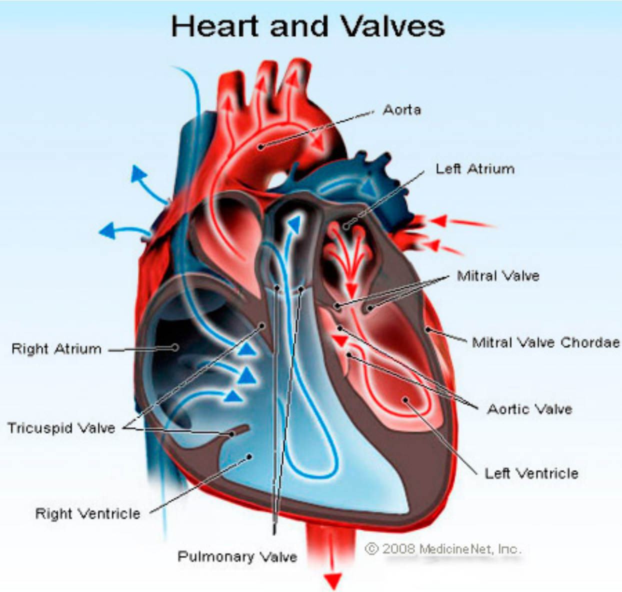
Heart and Valves
Aorta
Left Atrium
Mitral Valve
Mitral Valve Chordae
Right Atrium
Aortic Valve
Tricuspid Valve
Left Ventricle
Right Ventricle
Pulmonary Valve
© 2008 MedicineNet, Inc.

Aortic valve

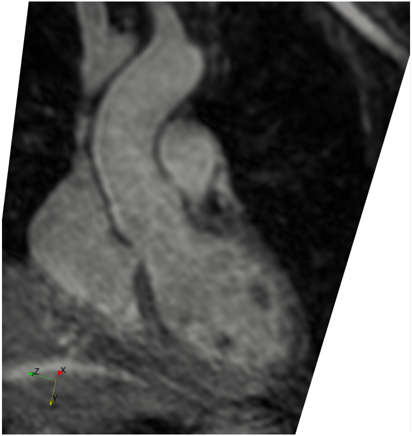

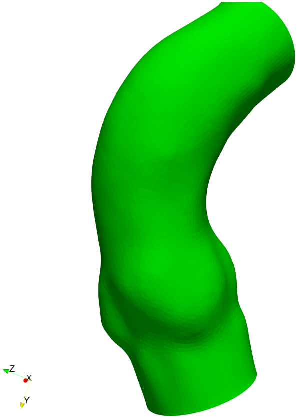

Aortic valve stenosis

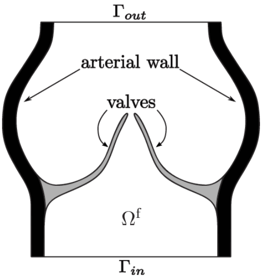

S. C. Shadden, M. Astorino and J-F. Gerbeau: Computational analysis of an aortic valve jet with Lagrangian coherent structures. In: Chaos: An Interdisciplinary Journal of Nonlinear Science 20.1 (2010):017512.

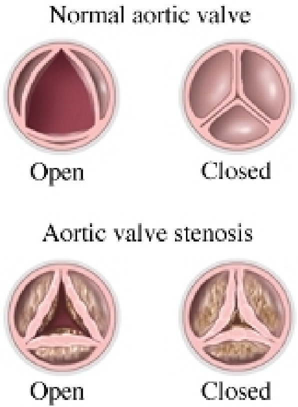

heartsurgeryinfo.com

Aortic valve stenosis evaluation

- anatomic stenosis

$$severity = \left(1 - \frac{area_{stenotic}}{area_{healthy}}\right) \cdot 100\%$$

- physiologically important stenosis
  - valve area/effective orifice area
  - additional heart work/energy dissipation
  - trans-stenosis pressure difference

Pressure difference

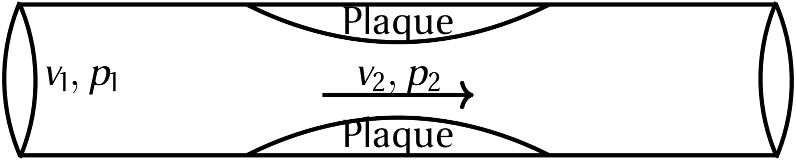

$$0.5\rho_* v_1^2 + h_1\rho_* g_* = 0.5\rho_* v_2^2 + h_2\rho_* g_* + E_{dis}$$

$$(h_1 - h_2)\rho_* g_* = 0.5\rho_* \left(v_2^2 - v_1^2\right) + E_{dis}$$

$$h_1 - h_2 = C v_2^2$$

R. Gorlin, S. Gorlin: Hydraulic formula for calculation of the area of the stenotic mitral valve, other cardiac valves, and central circulatory shunts. I. In: American Heart Journal, 41(1) (1951): 1–29.

Pressure Poisson equation

$$-\nabla p = \rho_* \left((\nabla\, \mathbf{v})\, \mathbf{v} + \frac{\partial \mathbf{v}}{\partial t} \right) - \mu_* \triangle \mathbf{v} =: \mathbf{f}$$

$$\begin{aligned}
-\Delta q_{\text{ppe}} &= \operatorname{div} \mathbf{f} && \text{in } \Omega \\
\frac{\partial q_{\text{ppe}}}{\partial \mathbf{n}} &= \mathbf{n} \cdot \mathbf{f} && \text{on } \partial\Omega \\
q_{\text{ppe}} &= p_* && \text{on } \Gamma_{out}
\end{aligned}$$

Stokes equation

$$-\nabla p = \rho_* \left((\nabla \mathbf{v})\, \mathbf{v} + \frac{\partial \mathbf{v}}{\partial t} \right) - \mu_* \triangle \mathbf{v} =: \mathbf{f}$$

$$\begin{aligned} -\Delta \mathbf{a} - \nabla q_{\mathrm{ste}} &= \mathbf{f} && \text{in } \Omega, \\ \operatorname{div} \mathbf{a} &= 0 && \text{in } \Omega, \\ \mathbf{a} &= 0 && \text{on } \partial\Omega, \\ q_{\mathrm{ste}} &= p_* && \text{on } \Gamma_{out}. \end{aligned}$$

H. Švihlová, J. Hron, J. Málek, K. R. Rajagopal, K. Rajagopal (2016): *Determination of pressure data from velocity data with a view toward its application in cardiovascular mechanics. Part 1. Theoretical considerations.* In: International Journal of Engineering Science 105,108–127.

Work-energy relative pressure estimator

$$\int_\Omega \rho_* \frac{\partial \mathbf{v}}{\partial t} \cdot \mathbf{v} \, dx + \int_\Omega \rho_* \left(\nabla \mathbf{v}\right) \mathbf{v} \cdot \mathbf{v} \, dx - \int_\Omega \mu_* \triangle \mathbf{v} \cdot \mathbf{v} \, dx + \int_\Omega \nabla p \cdot \mathbf{v} \, dx = 0$$

$$\frac{\partial K_e}{\partial t} + A_e + V_e + H(p) = 0$$

$$H(p) = \int_\Gamma p\mathbf{v} \cdot \mathbf{n} \, dS + \int_\Omega p \, \mathrm{div} \, \mathbf{v} \, dx = (p_{in} - p_{out}) \int_{\Gamma_{in}} \mathbf{v} \cdot \mathbf{n} \, dS$$

$$K_e = 0.5 \rho_* \int_\Omega \mathbf{v} \cdot \mathbf{v} \, dx$$

$$A_e = \rho_* \int_\Gamma (\mathbf{v} \cdot \mathbf{n}) (\mathbf{v} \cdot \mathbf{v}) \, dS - \rho_* \int_\Omega (\mathbf{v} \cdot \mathbf{v}) \, \mathrm{div} \, \mathbf{v} \, dx$$

$$V_e = - \int_\Gamma \mu_* \left(\nabla \mathbf{v}\right) \mathbf{n} \cdot \mathbf{v} \, dS + \int_\Omega \mu_* \nabla \mathbf{v} : \nabla \mathbf{v} \, dx$$

F. Donati, C. A. Figueroa, N. P. Smith, P. Lamata, D. A. Nordsletten: Non-invasive pressure difference estimation from PC-MRI using the workenergy equation. In: Medical Image Analysis, 26(1) (2015):159–172.

Virtual WERP

$$\int_\Omega \rho_* \frac{\partial \mathbf{v}}{\partial t} \cdot \mathbf{w}\, dx + \int_\Omega \rho_* \left(\nabla \mathbf{v}\right) \mathbf{v} \cdot \mathbf{w}\, dx + \\ - \int_\Omega \mu_* \triangle \mathbf{v} \cdot \mathbf{w}\, dx + \int_\Omega \nabla p \cdot \mathbf{w}\, dx = 0$$

$$\frac{\partial K_e}{\partial t} + A_e + V_e + H(p) = 0$$

$$H(p) = \int_\Gamma p\mathbf{w} \cdot \mathbf{n}\, dS + \int_\Omega p\ \mathrm{div}\, \mathbf{w}\, dx = \left(p_{in} - p_{out}\right) \int_{\Gamma_{in}} \mathbf{w} \cdot \mathbf{n}\, dS$$

$$K_e = 0.5 \rho_* \int_\Omega \mathbf{v} \cdot \mathbf{w}\, dx$$

$$A_e = \rho_* \int_\Gamma \left(\mathbf{w} \cdot \mathbf{n}\right) \left(\mathbf{v} \cdot \mathbf{v}\right)\ dS$$

$$V_e = - \int_\Gamma \mu_* \left(\nabla \mathbf{v}\right) \mathbf{n} \cdot \mathbf{w}\, dS + \int_\Omega \mu_* \nabla \mathbf{v} : \nabla \mathbf{w}\, dx$$

Virtual WERP

$$(p_{in} - p_{out}) \int_{\Gamma_{in}} \mathbf{w} \cdot \mathbf{n} \, dS = -\left(\frac{\partial K_e}{\partial t} + A_e + V_e \right)$$

$$\triangle \mathbf{w} + \nabla \lambda = 0$$

$$\operatorname{div} \mathbf{w} = 0$$

$$\mathbf{w} = 0 \text{ on } \Gamma_{wall}$$

$$\mathbf{w} = \mathbf{n} \text{ on } \Gamma_{in}$$

D. Marlevi, B. Ruijsink, M. Balmus, D. Dillon-Murphy, D. Fovargue, K. Pushparajah, C. Bertoglio, P. Lamata, C. A. Figueroa, R. Razavi, D. A. Nordsletten: Estimation of Cardiovascular Relative Pressure Using Virtual Work-Energy. In: Scientific Reports, 9(1) (2019).

Pressure estimators

Without noise

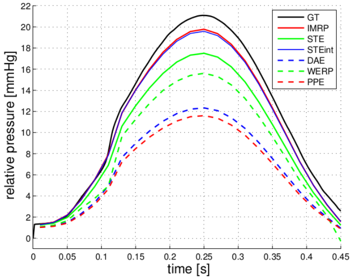

(a) $h = 0.15$ cm

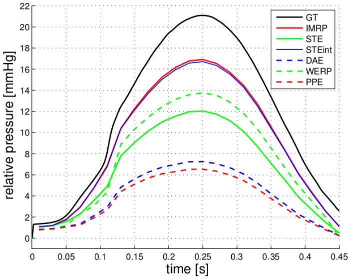

(b) $h = 0.25$ cm

C. Bertoglio, R. Nuñez, F. Galarce, D. Nordsletten, A. Osses: Relative pressure estimation from velocity measurements in blood flows: State-of-the-art and new approaches. In: International Journal for Numerical Methods in Biomedical Engineering, 34(2) (2017): e2925.

Pressure estimators

Including noise

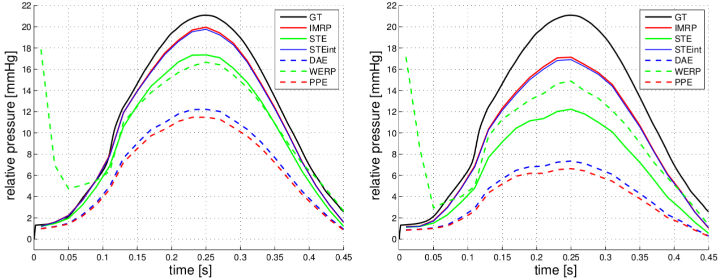

(a) $h = 0.15$ cm (b) $h = 0.25$ cm

C. Bertoglio, R. Nuñez, F. Galarce, D. Nordsletten, A. Osses: Relative pressure estimation from velocity measurements in blood flows: State-of-the-art and new approaches. In: International Journal for Numerical Methods in Biomedical Engineering, 34(2) (2017): e2925.

Aortic valve stenosis evaluation

Aortic root physiological flow

The impact of slip boundary conditions on aortic root vorticity

Da Vinci hypothesis

- the shape of the sinuses of Valsalva is required for aortic root vortices formation
  - B. J. Bellhouse, F. H. Bellhouse: Mechanism of Closure of the Aortic Valve. Nature, 217(5123) (1968): 86–87.

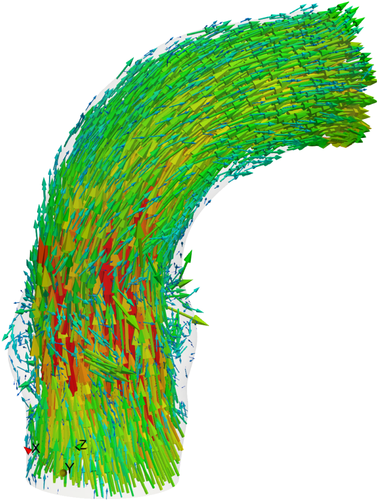

Da Vinci hypothesis

- the physiological functions of the vortices are required for normal aortic valve closure
  - T. E. David, S. Armstrong, C. Manlhiot, B. W. McCrindle, C. M. Feindel: Long-term results of aortic root repair using the reimplantation technique. In: The Journal of Thoracic and Cardiovascular Surgery, 145(3) (2013):S22–S25.

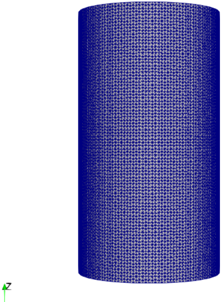

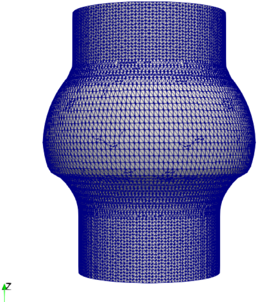

Input data/4D PC-MRI

- time resolved phase-contrast magnetic resonance imaging (4D PC-MRI or 4D Flow MRI)

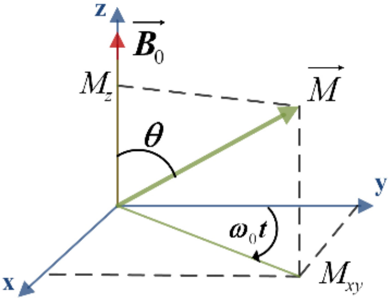

C. Coillot et al.: Signalmodeling of an MRI ribbon solenoid coil dedicated to spinal cord injury investigations. In: Journal of Sensors and Sensor Systems, Copernicus GmbH, 5 (2016): 137-145.

4D PC-MRI

Magnetization: (angular magnetic momentum) $\mathbf{M} = \mathbf{r} \times \mathbf{p}$
Lorentz Force Law: $\mathbf{F} = q\mathbf{v} \times \mathbf{B}$
Magnetic torque: $\frac{d\mathbf{M}}{dt} = \mathbf{r} \times \mathbf{F}$

$$\frac{d\mathbf{M}}{dt} = \mathbf{r} \times q\mathbf{v} \times \mathbf{B} = \mathbf{r} \times \frac{q}{m}\mathbf{p} \times \mathbf{B} = \gamma\left(\mathbf{M} \times \mathbf{B}\right)$$

Static field: $\mathbf{M} = (0, 0, M_0)$
RF-pulse: $\mathbf{M} \to (M_x, M_y, 0)$ for a very short time

$$\frac{dM_x}{dt} = \gamma(\mathbf{M} \times \mathbf{B})_x - \frac{M_x}{T_2}$$
$$\frac{dM_y}{dt} = \gamma(\mathbf{M} \times \mathbf{B})_y - \frac{M_y}{T_2}$$
$$\frac{dM_z}{dt} = \gamma(\mathbf{M} \times \mathbf{B})_z - \frac{(M_z - M_0)}{T_1}$$

T1 relaxation time (longitudial magnetization recovery)
T1 = time when 63% of the spins ale aligned with B_0

$$M_z(t) = M_0(1 - e^{-\frac{t}{T_1}})$$

T2 relaxation time (dephasing)
T2 = time when 63% of the spins are out of phase

$B_0 = 1.5T$	T1[ms]	T2[ms]
myocardium	950	55
arterial blood	1550	250
fat	260	110

4D PC MRI

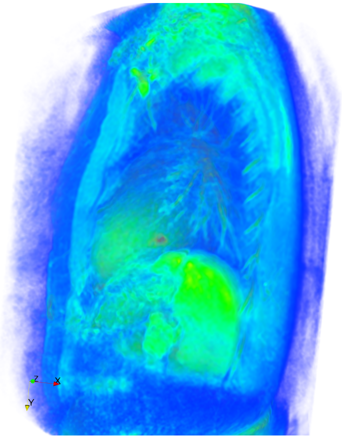

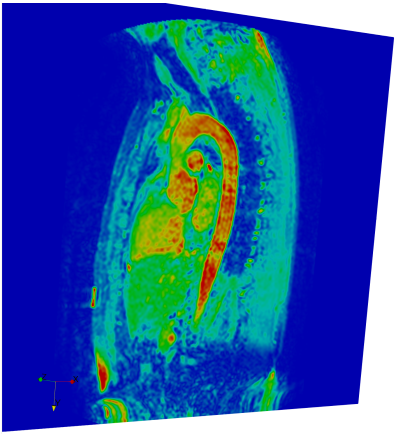

4D PC MRI

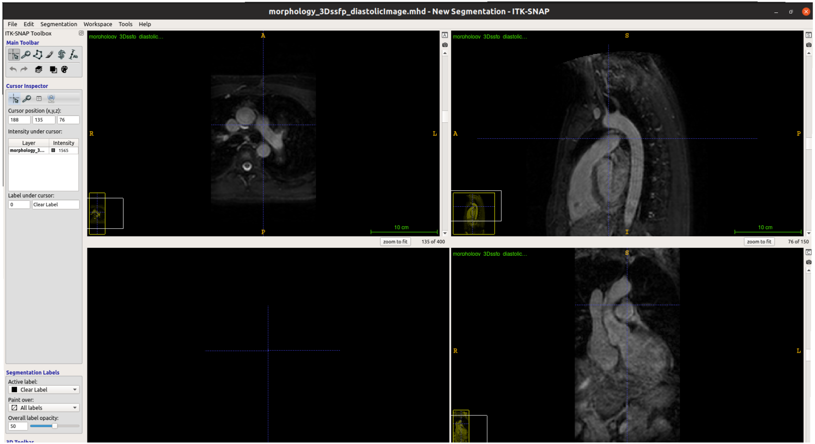
morphology_3Dssfp_diastolicImage.mhd - New Segmentation - ITK-SNAP
File Edit Segmentation Workspace Tools Help
ITK-SNAP Toolbox
Main Toolbar
Cursor Inspector
Cursor position (x,y,z):
188
135
76
Intensity under cursor:
Layer
Intensity
morphology_3...
1565
Label under cursor:
0
Clear Label
Segmentation Labels
Active label:
Clear Label
Paint over:
All labels
Overall label opacity:
50
3D Toolbar
10 cm
zoom to fit
135 of 400
76 of 150

4D PC MRI

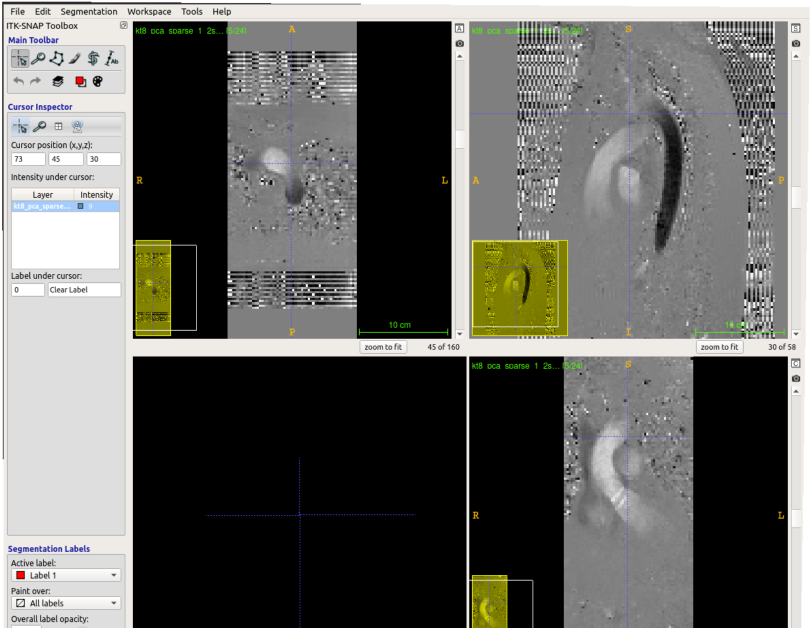

File Edit Segmentation Workspace Tools Help
ITK-SNAP Toolbox
Main Toolbar
Cursor Inspector
Cursor position (x,y,z):
73
45
30
Intensity under cursor:
Layer
Intensity
kt8_pca_sparse...
9
Label under cursor:
0
Clear Label
Segmentation Labels
Active label:
Label 1
Paint over:
All labels
Overall label opacity:
kt8 pca sparse 1 2s... [5/24]
A
R
L
P
10 cm
zoom to fit
45 of 160
S
I
30 of 58

4D PC MRI

- morphology file (metaimage format)
  - vs=1.05mm
  - f(i,j,k)=intensity; i,j=1,..,400, k=1,..,150
- 3x velocity component file (metaimage format)
  - vs=2.5mm, ts=30ms
  - f(t,i,j,k)=v_x; i,j,=1,..160, k=1,..,58, t=0,..,24
- segmentation and smoothing:
  - VMTK (vmtk.org) semi-automatic segmentation, meshing, smoothing
  - ITKSNAP (itksnap.org) manual and semi-automatic segmentation
  - iso2mesh (iso2mesh.sourceforge.net) smoothing, meshing
- registered files

$$\begin{pmatrix} x \\ y \\ z \end{pmatrix} = \begin{pmatrix} ox \\ oy \\ oz \end{pmatrix} + \begin{pmatrix} vs_x & 0 & 0 \\ 0 & vs_y & 0 \\ 0 & 0 & vs_z \end{pmatrix} \begin{pmatrix} r_{11} & r_{12} & r_{13} \\ r_{21} & r_{22} & r_{23} \\ r_{31} & r_{32} & r_{33} \end{pmatrix} \begin{pmatrix} i \\ j \\ k \end{pmatrix}$$

4D PC MRI

- morphology file (metaimage format)
  - vs=1.05mm
  - f(i,j,k)=intensity; i,j=1,..,400, k=1,..,150
- 3x velocity component file (metaimage format)
  - vs=2.5mm, ts=30ms
  - f(t,i,j,k)=v_x; i,j,=1,..160, k=1,..,58, t=0,..,24
- segmentation and smoothing:
  - VMTK (vmtk.org) semi-automatic segmentation, meshing, smoothing
  - ITKSNAP (itksnap.org) manual and semi-automatic segmentation
  - iso2mesh (iso2mesh.sourceforge.net) smoothing, meshing
- registered files

$$\begin{pmatrix} x \\ y \\ z \end{pmatrix} = \begin{pmatrix} -ox \\ -oy \\ oz \end{pmatrix} + \begin{pmatrix} vs_x & 0 & 0 \\ 0 & vs_y & 0 \\ 0 & 0 & vs_z \end{pmatrix} \begin{pmatrix} r_{11} & r_{12} & r_{13} \\ r_{21} & r_{22} & r_{23} \\ r_{31} & r_{32} & r_{33} \end{pmatrix} \begin{pmatrix} -i \\ j \\ -k \end{pmatrix}$$

4D PC MRI

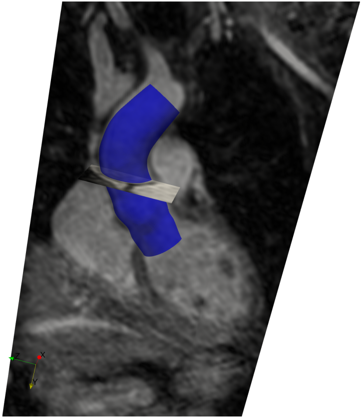

Z
X
Y

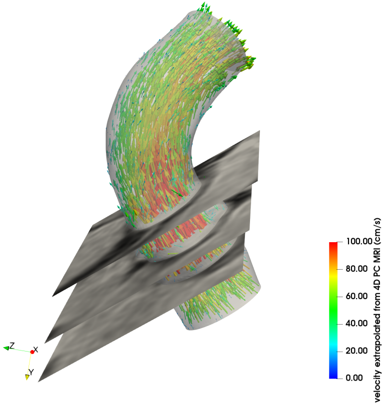

Z
X
Y
100.00
80.00
60.00
40.00
20.00
0.00
velocity extrapolated from 4D PC MRI (cm/s)

Aortic valve stenosis evaluation

Aortic root physiological flow

The impact of slip boundary conditions on aortic root vorticity

Vortex formation in stenotic valves

NO-SLIP 30% severity FREE-SLIP 30% severity

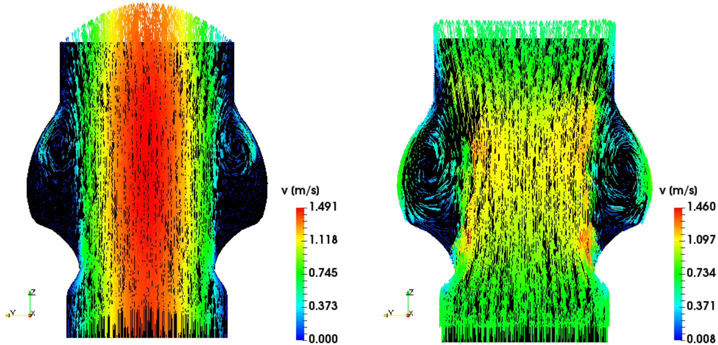

Figure: Velocity distribution on a slice of the valvular geometry with 30% severity in time of peak velocity.

Slip boundary condition

$$\operatorname{div} \mathbf{v} = 0$$

$$\rho_* \left(\frac{\partial \mathbf{v}}{\partial t} + (\nabla \mathbf{v}) \mathbf{v} \right) = \operatorname{div} \mathbf{T}$$

$$\mathbf{T} = -p\mathbf{I} + \mu_* \left(\nabla \mathbf{v} + \nabla \mathbf{v}^T \right)$$

$$\mathbf{v} \cdot \mathbf{n} = 0 \text{ and } \theta \mathbf{v}_\tau = \gamma_* (1 - \theta)(\mathbf{T}\mathbf{n})_\tau \qquad \text{on } \Gamma_{wall}$$

$$\mathbf{v} = -\overline{V(t)} \frac{4\mu_* R(1-\theta) + 2\theta(R^2 - \rho_X^2)}{4\mu_* R(1-\theta) + \theta R^2} \mathbf{n} \qquad \text{on } \Gamma_{in}$$

$$\mathbf{T}\mathbf{n} = -\frac{\overline{P(t)}}{\rho_*} \mathbf{n} + \frac{1}{2} (\mathbf{v} \cdot \mathbf{n})_- \mathbf{v} \qquad \text{on } \Gamma_{out}$$

Slip boundary condition

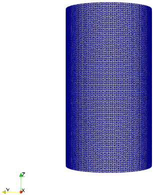

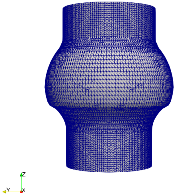

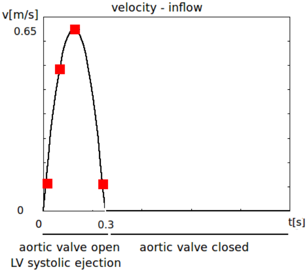

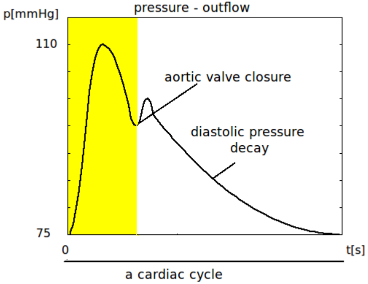

Slip boundary condition

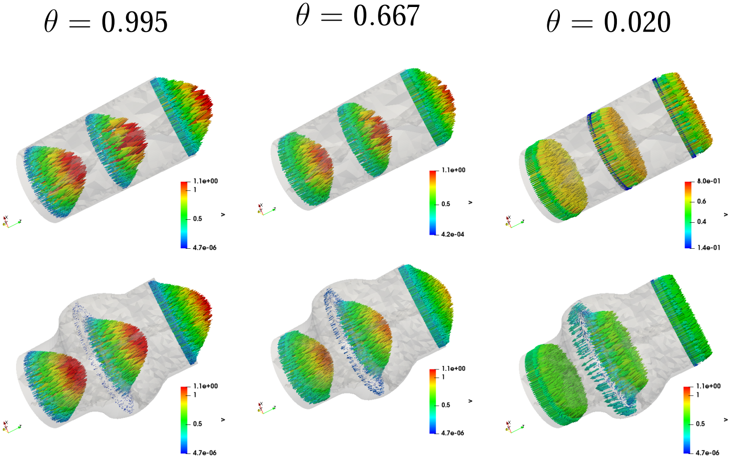

Slip boundary condition

mid-systole　peak velocity　late systole

$\theta = 0$

$\theta = 0.333$

$\theta = 0.500$

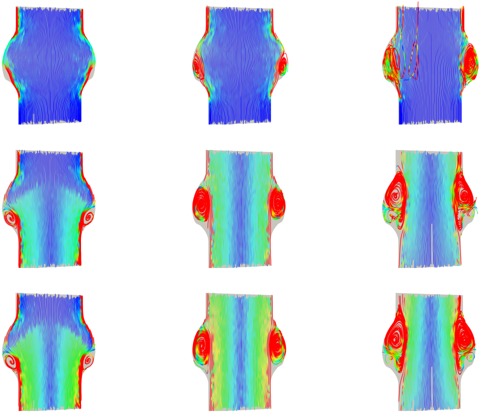

Slip boundary condition

mid-systole peak velocity late systole

$\theta = 0.666$

$\theta = 0.995$

$\theta = 1$

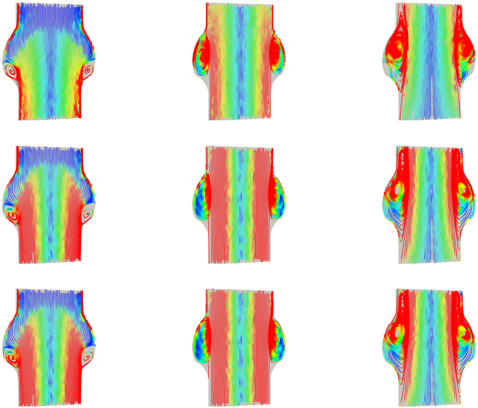

Comparison with 4D PC MRI data

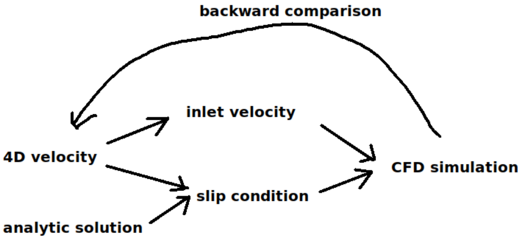

$$\mathbf{v} = -\overline{V(t)}\frac{4\mu_* R(1-\theta) + 2\theta(R^2 - \rho_X^2)}{4\mu_* R(1-\theta) + \theta R^2}\mathbf{n}$$

$$|\mathbf{v}| = -\overline{V(t)}\frac{4\mu_* R(1-\theta) + 2\theta R^2}{4\mu_* R(1-\theta) + \theta R^2} + \overline{V(t)}\frac{2\theta\rho_X^2}{4\mu_* R(1-\theta) + \theta R^2}$$

Comparison with 4D PC MRI data

estimated parameter	θ
descending aorta	0.42

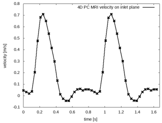

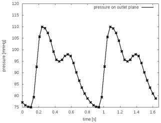

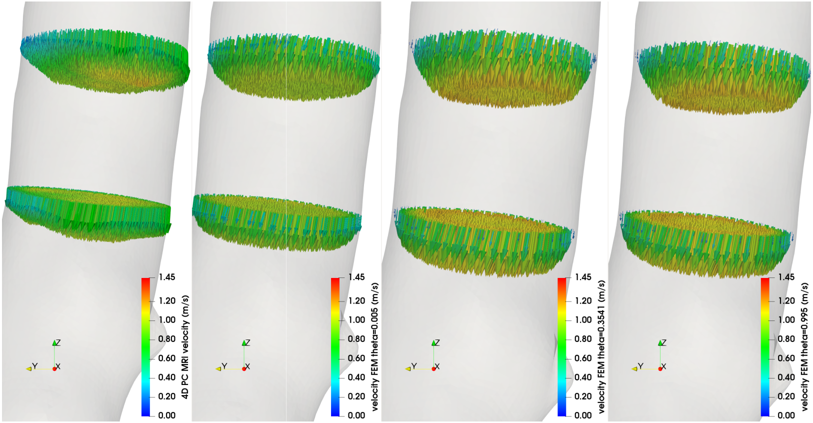

Comparison with 4D PC MRI data

estimated parameter	θ
descending aorta	0.42

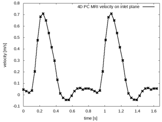

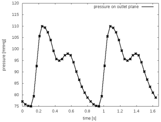

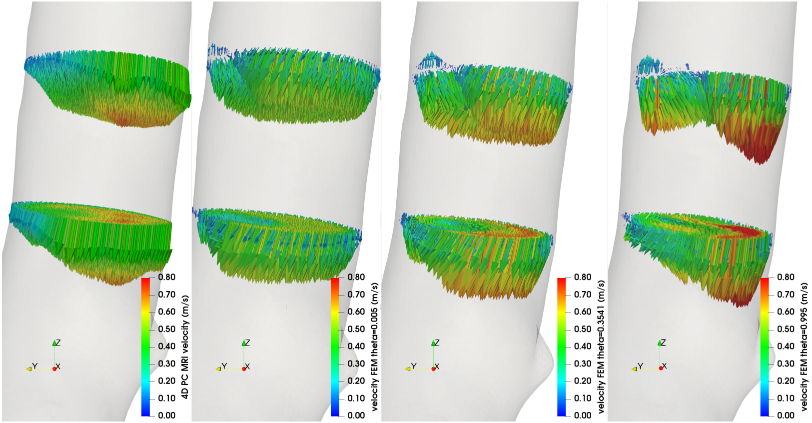

Comparison with 4D PC MRI data

estimated parameter	θ
aortic root base	0.63

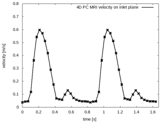

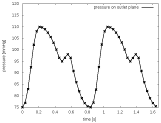

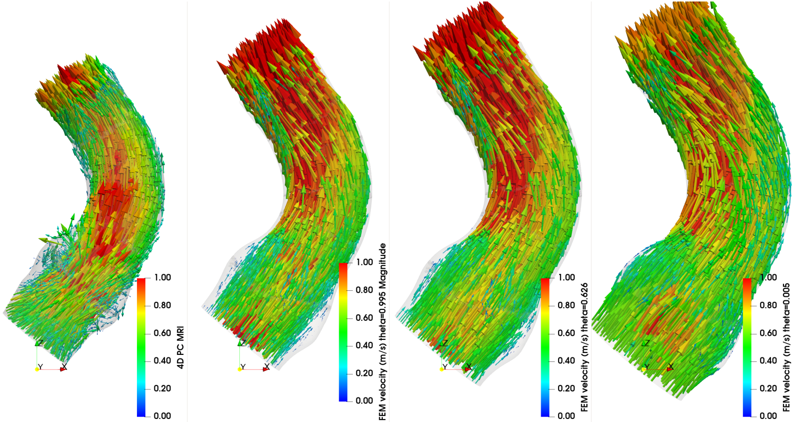

Comparison with 4D PC MRI data

estimated parameter	θ
aortic root base	0.63

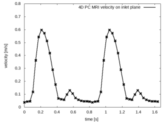

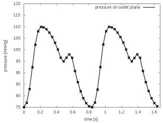

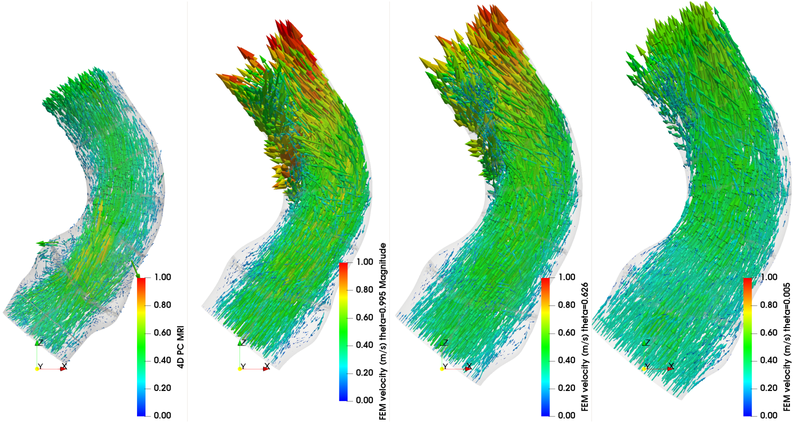

Partial volume effect and boundary extraction

- R. Fučík et al.: Investigation of phase-contrast magnetic resonance imaging underestimation of turbulent flow through the aortic valve phantom: Experimental and computational study using lattice Boltzmann method. In: Magnetic Resonance Materials in Physics, Biology and Medicine (2020).
- D. Nolte, C. Bertoglio: Reducing the impact of geometric errors in flow computations using velocity measurements. In: International Journal for Numerical Methods in Biomedical Engineering (2019): e3203.

Partial volume effect and boundary extraction

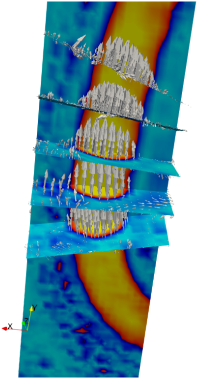

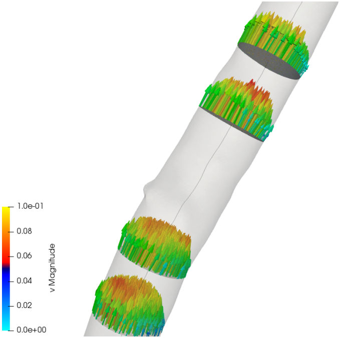

Conclusion - 3 goals and 3 messages

- we presented the state-of-art for models available to determine the pressure from the velocity field
- the magnetic resonance imaging data are now available
- there are still fundamental questions in blood flow modelling and blood flow imaging too

Thank you for your attention.